Frontiers of Physics
https://doi.org/10.1007/s11467-021-1084-7
Front. Phys.
16(5), 52503 (2021)

RESEARCH ARTICLE

Helicity-dependent time delays in multiphoton ionization by two-color circularly polarized laser fields

Qing-Hua Ke[1], Yue-Ming Zhou[1,†], Yi-Jie Liao[1], Jin-Tai Liang[1], Yong Zhao[1], Jia Tan[1], Min Li[1], Pei-Xiang Lu[1,2,3,‡]

[1] *School of Physics and Wuhan National Laboratory for Optoelectronics, Huazhong University of Science and Technology, Wuhan 430074, China*
[2] *Hubei Key Laboratory of Optical Information and Pattern Recognition, Wuhan Institute of Technology, Wuhan 430205, China*
[3] *CAS Center for Excellence in Ultra-intense Laser Science, Shanghai 201800, China*
Corresponding authors. E-mail: †zhouymhust@hust.edu.cn, ‡lupeixiang@hust.edu.cn
Received March 4, 2021; accepted May 8, 2021

By numerically solving the three-dimensional time-dependent Schrödinger equation, we have investigated multiphoton ionization of hydrogen atom in the two-color circularly polarized (TCCP) laser fields consisting of a strong 400 nm and a much weaker 800 nm pulses. Due to the presence of perturbative 800 nm laser pulse, sideband peaks emerge between the above-threshold ionization rings in the photoelectron momentum distributions. Our numerical results show that the sideband peaks exhibit one-lobe structure in the co-rotating TCCP laser fields, while it displays the three-lobe structure in the counter-rotating TCCP laser fields. Moreover, the photoelectron yield of sidebands in the co-rotating TCCP fields is much higher than those of the counter-rotating TCCP fields. These phenomena could be well explained from the perspective of the photon-absorption channels via the selection rules. Interestingly, an obvious phase shift between the sidebands of different orders from the co-rotating and counter-rotating TCCP fields is observed. This shift indicates the helicity-dependent time delay in the one-photon continuum-continuum transition process.

Keywords helicity-dependent time delay, TCCP, multiphoton ionization

1 Introduction

The development of coherent extreme-ultraviolet (XUV) attosecond laser pulses makes it possible to resolve electronic dynamic on an unprecedented time scale. Attosecond pulse trains (APT), in the presence of weak infrared (IR) laser pulses, is a very promising tool to conduct time-resolved experiments, known as reconstruction of attosecond beating by interference of two-photon transition (RABITT) technique [1–8]. In the typical RABITT experiments [1, 2], the sideband signals exhibit a cosine modulation as a function of the time delay between APT and IR laser fields. These modulations of different order sidebands reveal the phase shift, encoding the time delay information of the photoionization dynamics [7].

In recent years, the photoemission time delay in various atoms or molecules has been theoretically [9–12] and experimentally [7, 8, 13–17] investigated using the RABITT interferometric technique. For instance, the difference in time delay of tens of attoseconds between the electrons emitted from the 3s and 3p subshell of argon has been measured [7]. Very recently, the angular-resolved RABITT technique has been developed [16–20]. The anisotropic photoemission time delay has been measured in the presence of the autoionizing states [15, 16]. Molecular stereo Wigner time delay has also been demonstrated by the orientation- and energy-resolved experiments [14]. The time delay in the typical RABITT experiments generally consists of three parts [8, 9], the group delay of the XUV field, the Wigner or intrinsic time delays and the continuum-continuum (c–c) delay τ_{cc}. In most previous works, attention was paid to the intrinsic time delay, while it was approximately that the c–c delay was universal and it can be eliminated. Recently, the c–c time delay has attracted more and more interest [21, 22]. The scheme by comparison of two measurements with different orders of c–c transitions was proposed to extract phase information on c–c couplings [21]. The dependence of the time delay on angular quantum number of the liberated photoelectron in the one-photon transition between continuum states has been experimentally quantified, and a time delay of 12 attoseconds between outgoing s and d electrons has been measured using the RABITT technique [22].

* arXiv: 2105.10151. This article can also be found at http://journal.hep.com.cn/fop/EN/10.1007/s11467-021-1084-7.

© Higher Education Press 2021

This two-photon transition interferometric technique has been extended to multiphoton regime [23–25] in past years. In Ref. [23], a phase measurement technique similar to the RABITT technique was proposed to probe the intrinsic delay in above threshold ionization (ATI), where the combination of a strong 400 nm and a weak 800 nm linearly polarized laser pulses was employed. In that scheme, the electron absorbs several 400 nm photons to reach the ATI peaks and subsequently absorbs or emits one 800 nm photon to reach sideband peaks. According to the selection rule, the angular quantum number of the electron could change by ±1 when the electron absorbs one linearly polarized photon, and thus the mixture of the angular quantum numbers at the ATI and sideband peaks is complex. It prevents us from studying the details of the time delay in the multiphoton ionization region. This problem could be avoided by employing the circularly polarized pulses. In the circularly polarized laser pulses, only one photon-absorption channel where the angular quantum number of the electron increases by one for the electron starting from the s state is allowed, while the other channel where the angular quantum number decreases by one is forbidden due to the selection rule. Thus, the mixture of the angular quantum numbers in the ATI and sideband peaks is relatively simpler compared to the case of linear laser pulses. As a consequence, the electron could reach a very high angular quantum number in the multiphoton region. This provides us a way to study the time delay of the electron with high angular quantum number, in contrast to previous RABITT experiments where only the s, p and d partial waves have been reached in the two-photon process. For the electron with high angular quantum numbers, the contribution of the short-range potential to the scattering phase is negligible, and thus the measured time delay is mainly attributed to the c–c transition process. This provides us a clean way to survey the angular momentum dependence of the c–c time delay, which is usually assumed to be independent on the angular momentum in previous studies.

In this paper, we have performed a theoretical study on multiphoton ionization of hydrogen atom by the two-color circularly polarized (TCCP) laser fields which consists of a strong 400 nm and a perturbative 800 nm laser fields. We should mention that the TCCP laser fields have been widely used in the strong-field ionization [26–35]. In our study, the 800 nm laser field is very weak and thus only one 800 nm photon is exchanged between the ATI peaks of the 400 nm laser field. This enables us to study the dynamics of the one-photon continuum-continuum transition. Our numerical results reveal two properties of the sidebands in the TCCP laser fields. The sidebands exhibit the one-lobe structure in the co-rotating laser fields, while the sidebands show the three-lobe structure in the counter-rotating laser fields. Moreover, the sideband yields in the co-rotating laser fields are much stronger than those in the counter-rotating TCCP laser fields. More interestingly, the maxima of sideband intensities at different orders show different relative shift, which is dependent on the helicity of TCCP laser fields. This shift difference is attributed to the c–c phase difference dependent on the angular quantum numbers. Throughout this paper, atomic units (a.u.) are used unless otherwise noted.

2 Numerical methods

In this paper, the photoelectron momentum distributions are obtained by numerically solving the three-dimensional (3D) time-dependent Schödinger equation (TDSE). It reads

$$\mathrm{i}\frac{\partial\psi(\boldsymbol{r},t)}{\partial t} = H(\boldsymbol{r},t)\psi(\boldsymbol{r},t), \tag{1}$$

where

$$H(\boldsymbol{r},t) = -\frac{1}{2}\nabla^2 - \frac{1}{r} - \mathrm{i}\boldsymbol{A}(t)\cdot\nabla. \tag{2}$$

∇ is the gradient operator. $\boldsymbol{A}(t)$ is the vector potential in dipole approximation, and it consists of two components:

$$\begin{aligned} A_x(t) &= -f(t)[A_1\cos(\omega_1 t) + A_2\cos(\omega_2 t + \Delta\phi)], \\ A_y(t) &= f(t)[A_1\sin(\omega_1 t) + \epsilon A_2\sin(\omega_2 t + \Delta\phi)]. \end{aligned} \tag{3}$$

Here, $\omega_1(\omega_2)$ is the angular frequency of 400 (800) nm laser field and $A_1(A_2)$ is the amplitude of the vector potential. A sine-square envelope $f(t)$ is adopted with a duration time of $30T_1$ ($T_1 = 2\pi/\omega_1$). The intensities of the 400 nm and perturbative 800 nm circularly polarized laser pulses are 3×10^{13} W/cm^2 and 1×10^{11} W/cm^2, respectively. $\epsilon = 1$ ($\epsilon = -1$) represents co-rotating (counter-rotating) TCCP laser fields with same (opposite) helicity. The relative phase $\Delta\phi$ of the two circularly polarized laser fields ranges from 0 to 2π separated by $\pi/40$.

The 3D-TDSE in Eq. (1) is solved in the spherical coordinate, where the wavefunction $\psi(\boldsymbol{r},t)$ can be expanded by spherical harmonics $|l,m\rangle$

$$|\psi(\boldsymbol{r},t)\rangle = \sum_{l,m}\frac{R_{lm}(r,t)}{r}|l,m\rangle. \tag{4}$$

Here, $R_{lm}(r,t)$ is the radial part of wavefunction, which is discretized by a finite-element discrete variable representation method [36]. The time propagation of the TDSE is calculated by the split-Lanczos method [37, 38] with the time step of $\Delta t = 0.1$ a.u.

The ionization amplitudes are obtained from the final wavefunction by projecting it to the scattering state $|\psi_{\boldsymbol{k}}(\boldsymbol{r})\rangle$ of hydrogen atom,

$$M(\boldsymbol{k}) = \langle\psi_{\boldsymbol{k}}(\boldsymbol{r})|\psi(\boldsymbol{r},t)\rangle. \tag{5}$$

The scattering state is given by

$$\psi_{\boldsymbol{k}}(\boldsymbol{r}) = \frac{1}{k}\frac{1}{\sqrt{2\pi}}\sum_{l,m}\mathrm{i}^l\mathrm{e}^{-\mathrm{i}(\sigma_l+\delta_l)}Y^*_{l,m}(\hat{k})R_{kl}(r)Y_{lm}(\hat{r}), \tag{6}$$

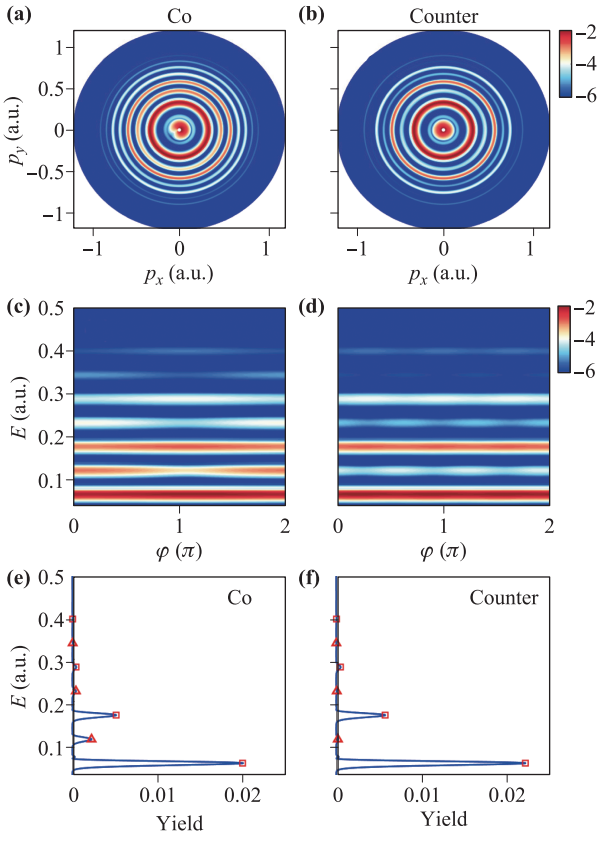


Fig. 1 **(a, b)** The PEMDs (logarithmic scale) of polarization plane. **(c, d)** The angular-resolved energy spectra. **(e, f)** The angular-integrated energy spectra. The ATI and sideband peaks are marked by square and triangle, respectively. The angle φ is the polar angle with $\varphi = 0$ along $+p_x$ direction. The intensities of 400 nm and 800 nm circularly polarized laser pulses are 3×10^{13} W/cm^2 and 1×10^{11} W/cm^2, respectively. The relative phase of the TCCP laser fields is $\Delta\phi = 0$.

where $\sigma_l = \arg\Gamma(l+1-\mathrm{i}Z/k)$ is the Coulomb phase shift, Z is the effective nuclear charge. The short-range induced phase shift $\delta_l = 0$ for the hydrogen atom.

The energy spectra ($E = |\boldsymbol{k}|^2/2$) are given by

$$D(E) = \int_0^{\pi} \sin\theta \mathrm{d}\theta \int_0^{2\pi} \mathrm{d}\varphi |M(\boldsymbol{k})|^2 |\boldsymbol{k}|. \tag{7}$$

In our numerical simulations, the maximal box size for radial coordinates is $R_{\max} = 200$ a.u., and the absorbing boundary is $R_c = 120$ a.u. The number of partial waves in Eq. (4) is limited to $L_{\max} = 35$ which ensures convergence of the calculations.

3 Numerical results and discussion

3.1 Numerical results

Figures 1(a) and (b) show the photoelectron momentum distributions (PEMD) in the polarization plane by the co-rotating and counter-rotating TCCP laser pulses, respectively. The intensity of the 400 nm laser pulse is 3×10^{13} W/cm^2, and it is 1×10^{11} W/cm^2 for the 800 nm laser field. The relative phase is $\Delta\phi = 0$. The presence of the perturbative 800 nm pulses leads to the sideband peaks between the ATI peaks in the PEMDs. To see the sideband peaks more clearly, the angular-resolved photoelectron energy spectra are presented in Figs. 1(c) and (d). By comparing the sidebands in the PEMDs by the co-rotating [Figs. 1(c)] and counter-rotating [Fig. 1(d)] TCCP fields, two phenomena are revealed. First, the sidebands in Fig. 1(c) have only one maximum, while the sidebands in Fig. 1(d) have three maxima. Second, the sideband yields in Fig. 1(c) are much stronger than those of the same orders in Fig. 1(d). The latter phenomenon is more clearly presented in the angular-integrated energy spectra in Figs. 1(e) and (f). In Fig. 1(e), there are small sideband peaks (triangle) between ATI peaks (square), while the sideband peaks in Fig. 1(f) are difficult to distinguish in the linear scale. This phenomenon has been reported in a recent experiment [39], wherein the dependence of sideband intensity on the relative helicity of the TCCP laser fields was explained by the modulation of sub-cycle interference. In this study, we will explain these phenomena from the perspective of the absorption channels. We note that the structures adjacent to the ATI peaks can be mainly attributed to the effects of the laser field envelope [40, 41].

Closer inspection of Fig. 1(d) shows the relative shift among the maxima of different order of the sidebands. To investigate this relative shift, Fig. 2 presents photoelectron energy spectra cut from the PEMDs at $\varphi = \pi$ as a function of the relative phase $\Delta\phi$. Different orders of the ATI and sideband peaks are labeled at the right side in Fig. 2. The photoelectron yields of sideband peaks oscillate with respect to the relative phase [42]. To quantitatively show the oscillation of sideband peaks, Fig. 3 presents the slices (circle) at sideband peaks in Fig. 2 as a function of the relative phase $\Delta\phi$. For comparison, the slices of the 4th-order ATI peaks (bottom panel) is

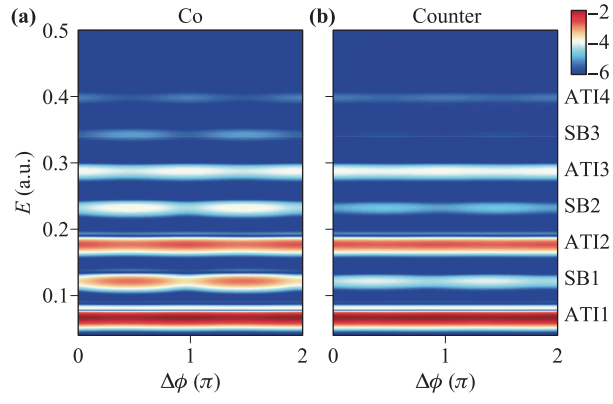


Fig. 2 The energy spectra cut at $\varphi = \pi$ in the co-rotating **(a)** and counter-rotating **(b)** TCCP laser fields as a function of the relative phase $\Delta\phi$.

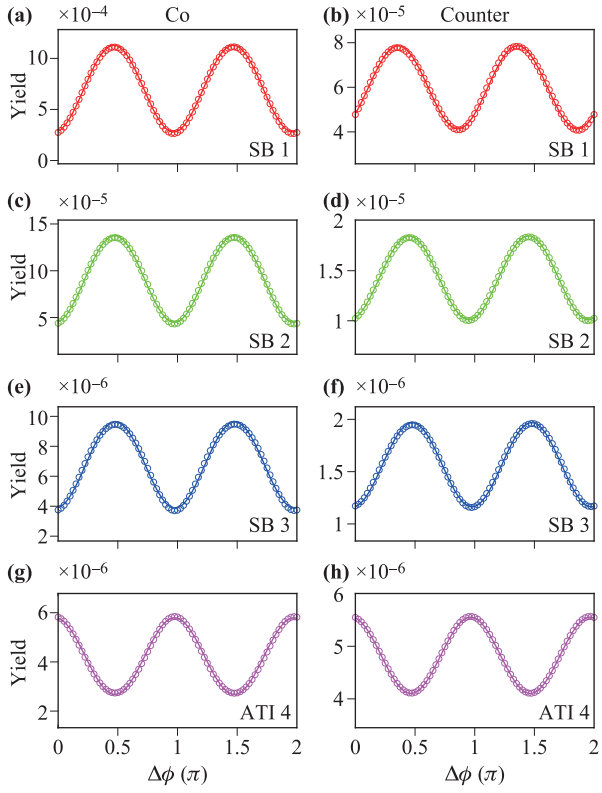


Fig. 3 The slices of the sideband and ATI peaks in Fig. 2 as a function of relative phase. The left and right panel are results of the co-rotating and counter-rotating TCCP lasers fields, respectively. The bottom panel is the 4th-order ATI yields. The circles are the TDSE results and the solid lines are fitting curves.

also shown in Fig. 3. The relative shift of sideband yield maxima in the counter-rotating TCCP laser pulses (right panel) is revealed. While the relative shift of sideband yield maxima in the co-rotating TCCP laser pulses (left panel) is much smaller.

3.2 Discussion

To explain the phenomena above, Fig. 4 shows the scheme of multiphoton ionization of hydrogen atom by the TCCP laser pulses. For the TCCP fields in this study, where the 800 nm component is very weak, the ionization dynamics can be approximately considered as two-step process. First, the electron in the ground state 1 s of hydrogen atom absorbs several 400 nm photons to reach the ATI peaks. Subsequently, the electron in the ATI peaks exchanges one co-rotating or counter-rotating 800 nm photon to reach the sidebands. Note that the absorbing of the 400 nm photon is the same for the co-rotating and counter-rotating TCCP fields.

The angular and magnetic quantum number (l, m) (with $l = m$) of the electron at ATI peaks are presented at the right side in Fig. 4. Due to the perturbative intensities of 800 nm laser fields, only one-photon transition

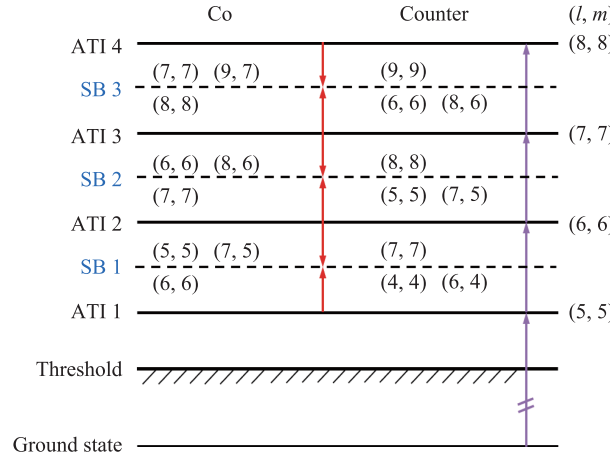


Fig. 4 The multiphoton ionization scheme of H atom by the TCCP laser pulses. The electron absorbs several photons of 400 nm and subsequently exchanges a photon of 800 nm, reaching ATI and sideband peaks. The numbers at right side are angular and magnetic quantum number (l, m) of the electron reaching this ATI peak. The absorption and emission channels to sidebands are presented below and above the dashed lines.

from ATI peaks to sidebands is considered. When the electron absorbs one co-rotating or counter-rotating 800 nm photon from ATI peaks to sideband peaks, the magnetic quantum number changes $\Delta m = 1$ or $\Delta m = -1$, respectively. For the sideband peak between the lower ATI peak (l, m) and upper ATI peak $(l + 1, m + 1)$, there are three channels. In the co-rotating case, there are one absorption channel $(l + 1, m + 1)$ and two emission channels (l, m), $(l + 1, m)$. While in the counter-rotating case, there are two absorption channels $(l + 1, m - 1)$, $(l - 1, m - 1)$ but one emission channel $(l + 2, m + 2)$. The quantum numbers (l, m) of the emission and absorption channels are represented above and below dashed lines in Fig. 4, respectively.

In the co-rotating case, the photoionization amplitude at the sideband peaks is [9, 22, 43]

$$A_{\rm co} = A^{(+)}_{l+1,m+1} Y^{m+1}_{l+1} + A^{(-)}_{l,m} Y^{m}_{l} + A^{(-)}_{l+2,m} Y^{m}_{l+2}, \tag{8}$$

where (+) and (−) stand for the absorption channels from the lower ATI peak (l, m) and the emission channels from the upper ATI peak $(l + 1, m + 1)$, respectively. While for the counter-rotating TCCP laser pulses, it reads

$$\begin{aligned} A_{\rm counter} = {} & A^{(+)}_{l-1,m-1} Y^{m-1}_{l-1} + A^{(+)}_{l+1,m-1} Y^{m-1}_{l+1} \\ & + A^{(-)}_{l+2,m+2} Y^{m+2}_{l+2}, \end{aligned} \tag{9}$$

Here, the transition amplitude

$$A^{(\pm)}_{l,m} = |A_{l,m}| \exp[{\rm i}(\varphi^{(\pm)}_{l} \pm \omega_2 \tau)], \tag{10}$$

where $|A_{l,m}|$ is the modulus of transition amplitude and $\tau = \Delta\phi/\omega_2$. The phase of the one-photon matrix element

Table 1 Angular integrals of transition amplitudes from ATIs to sidebands. (l, m) is the angular momentum and magnetic number of this channel. $\pm$ represent absorption from the lower ATI (l, m) or emission from the upper ATI $(l+1, m+1)$.

Co	$(l+1, m+1, +)$	$(l, m, -)$	$(l+2, m, -)$
SB 1	0.4804	0.4804	0.0506
SB 2	0.4830	0.4830	0.0443
SB 3	0.4851	0.4851	0.0393
Counter	$(l-1, m-1, +)$	$(l+1, m-1, -)$	$(l+2, m+2, -)$
SB 1	0.4767	0.0591	0.4830
SB 2	0.4804	0.0506	0.4851
SB 3	0.4830	0.0443	0.4867

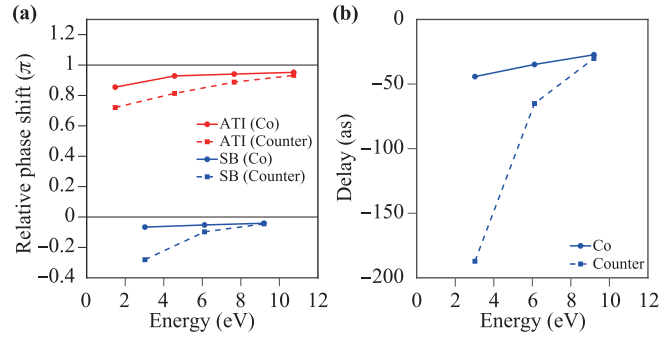


Fig. 5 **(a)** The retrieved relative phase shift of ATI (red) and sideband (blue) peaks. **(b)** The retrieved time delay $\delta_i/(2\omega_2)$ $(i = 1, 2)$.

has two parts [22, 23],

$$\varphi_l^{(\pm)} = \varphi_{<}^{\mathrm{ATI}}{}_{>} + \varphi_l^{\mathrm{cc}\pm}, \tag{11}$$

where $\varphi_{<}^{\mathrm{ATI}}{}_{>}$ represents the total phase of the multiphoton transition from bound state to the lower $(<)$ or upper $(>)$ ATI peak, and $\varphi_l^{\mathrm{cc}\pm}$ is the c–c transition phase induced by the transition from ATI peaks to sideband peaks.

From Eq. (8), there are two emission channels in the co-rotating TCCP laser fields. The angular integral in Table 1 of the amplitude for the transition from the ATI peaks to the sideband is described by the products of two Clebsch–Gordan coefficients [46]. From table 1, the angular integral of the emission channel (l, m) is about one-order larger than the other emission channel $(l+2, m)$. Hence, the channel (l, m) is the dominant emission channels in the co-rotating TCCP laser fields. Similarly, in the counter-rotating TCCP laser fields, the absorption channel $(l-1, m-1)$ dominates. The sideband probabilities in the polarization plane are thus approximately reduced to [22, 23]

$$\begin{aligned} I(E_f, \varphi, \Delta\phi) &\approx \begin{cases} |A_{l+1,m+1}^{(+)} Y_{l+1}^{m+1} + A_{l,m}^{(-)} Y_l^m|^2, \\ |A_{l-1,m-1}^{(+)} Y_{l-1}^{m-1} + A_{l+2,m+2}^{(-)} Y_{l+2}^{m+2}|^2, \end{cases} \\ &\propto \begin{cases} c_{11} + c_{12}\cos(\delta_1 + \varphi + 2\Delta\phi), & \text{Co} \\ c_{21} + c_{22}\cos(\delta_2 - 3\varphi + 2\Delta\phi). & \text{Counter} \end{cases} \end{aligned} \tag{12}$$

Here, c_{11}, c_{12}, c_{21} and c_{22} are the parameters related to the modulus of the transition amplitude. The phase shifts δ_1 and δ_2 are

$$\begin{aligned} \delta_1 &= \varphi_{<}^{\mathrm{ATI}} - \varphi_{>}^{\mathrm{ATI}} + \varphi_{l+1}^{\mathrm{cc}+} - \varphi_l^{\mathrm{cc}-}, \\ \delta_2 &= \varphi_{<}^{\mathrm{ATI}} - \varphi_{>}^{\mathrm{ATI}} + \varphi_{l-1}^{\mathrm{cc}+} - \varphi_{l+2}^{\mathrm{cc}-}. \end{aligned} \tag{13}$$

From Eq. (12), in the co-rotating case, the magnetic quantum number difference between the absorption and emission channels is $\delta m = 1$, which explains the angular one-lobe structure of the sidebands in Fig. 1(c). While in the counter-rotating case, this difference is $\delta m = 3$, and thus the sideband yields reveal the three-lobe structures in Fig. 1(d).

According to the Fano's propensity rule [44, 45], for the sideband yields, the absorption channel $(l+1, m+1)$ in the co-rotating TCCP laser fields is stronger than the channel $(l-1, m-1)$ in the counter-rotating TCCP laser fields. Similarly, the emission channel (l, m) in co-rotating case is also stronger than the channel $(l+2, m+2)$ in counter-rotating case. As a result, the sideband yields in the co-rotating TCCP laser fields is much stronger than those in the counter-rotating TCCP laser fields in Fig. 1.

Equation (12) indicates that the sideband yields exhibit a cosine modulation as a function of the relative phase $\Delta\phi$ with φ fixed. The signals of sidebands in Fig. 3 are well fitted (solid lines) by Eq. (12) using the genetic algorithm [47]. This implies that the higher-frequency contribution is negligible and it is reasonable for only considering one-photon transition between continuum states in our cases. The fitted phase shifts δ_i of both ATI and sideband peaks are shown in Fig. 5(a). The phase shift of sideband peaks increases as the photoelectron energy increases and approaches to 0 in both the co-rotating and counter-rotating cases. But the phase shift difference between the co-rotating and counter-rotating TCCP laser fields are clearly revealed in Fig. 5(a). The phase shift of sidebands in the co-rotating case shows little variation around 0, while it reaches about -0.3π at the lowest-order of sideband in the counter-rotating case. The interaction phase [48] is not observed in our results in Fig. 5(a). The phase shift in both the co-rotating and counter-rotating cases consists of two parts in Eq. (13). The first part is the bound to ATI peak phase difference $\varphi_{<}^{\mathrm{ATI}} - \varphi_{>}^{\mathrm{ATI}}$. This part is difficult to deal with in the multiphoton process but it is the same for the co-rotating and counter-rotating cases as stated before. The second contribution is the c–c phase difference $\varphi_{\mathrm{cc}}^{+} - \varphi_{\mathrm{cc}}^{-}$. The phase shift difference between the co-rotating and counter-rotating cases is thus attributed to the c–c phase dependent on the angular quantum numbers. In the counter-rotating case, the angular quantum number difference of the inter-

ference channels is $\delta l = 3$, leading to a larger c–c phase difference, while it is $\delta l = 1$ in the co-rotating case. This interpretation of the dependence of the c–c phase on the angular quantum numbers is further supported by a very recent article [49]. The corresponding time delay $\delta_i/(2\omega_2)$ $(i = 1, 2)$ of sidebands retrieved from the TDSE results is presented in Fig. 5(b). The time delay difference between two cases reaches about 150 as at the lowest-order sideband and it decreases with the increase of the sideband order. This time delay difference in multiphoton regime between the TCCP laser fields with same and opposite helicities has not been reported in previous studies.

4 Conclusions

In conclusion, we have theoretically investigated multiphoton ionization of H atom by solving the 3D-TDSE using 400 nm combined with co-rotating and counter-rotating perturbative 800 nm TCCP laser fields. The sideband signals present the one-lobe and three-lobe structures in the co-rotating and counter-rotating TCCP laser fields, respectively. Moreover, the sideband signals in co-rotating TCCP laser fields is much stronger than those of counter-rotating TCCP laser pulses. These phenomena have been explained with the absorption channels.

Interestingly, the modulations of sideband yields in the counter-rotating TCCP laser fields exhibit a visible phase shift, compared to those in the co-rotating TCCP laser pulses. It is mainly attributed to the one-photon continuum-continuum phase difference dependent on the angular quantum numbers.

Acknowledgements This work was supported by the National Key Research and Development Program of China (Grants No. 2019YFA0308300) and the National Natural Science Foundation of China (Grant Nos. 11874163 and 12021004).

References

1. P. M. Paul, E. S. Toma, P. Breger, G. Mullot, F. Auge, Ph. Balcou, H. G. Muller, and P. Agostini, Observation of a train of attosecond pulses from high harmonic generation, *Science* 292(5522), 1689 (2001)
2. E. S. Toma and H. G. Muller, Calculation of matrix elements for mixed extreme-ultraviolet-infrared two-photon above-threshold ionization of argon, *J. Phys. B* 35(16), 3435 (2002)
3. H. G. Muller, Reconstruction of attosecond harmonic beating by interference of two-photon transitions, *Appl. Phys. B* 74(S1), s17 (2002)
4. A. Maquet and R. Taïeb, Two-colour IR + XUV spectroscopies: The "soft-photon approximation", *J. Mod. Opt.* 54(13–15), 1847 (2007)
5. M. Swoboda, J. M. Dahlstrom, T. Ruchon, P. Johnsson, J. Mauritsson, A. L'Huillier, and K. J. Schafer, Intensity dependence of laser-assisted attosecond photo ionization spectra, *Laser Phys.* 19(8), 1591 (2009)
6. G. Laurent, W. Cao, H. Li, Z. Wang, I. Ben-Itzhak, and C. L. Cocke, Attosecond control of orbital parity mix interferences and the relative phase of even and odd harmonics in an attosecond pulse train, *Phys. Rev. Lett.* 109(8), 083001 (2012)
7. K. Klünder, J. M. Dahlstrom, M. Gisselbrecht, T. Fordell, M. Swoboda,D. Guenot, P. Johnsson, J. Caillat, J. Mauritsson, A. Maquet, R. Taieb, andA. L'Huillier, Probing single-photon ionization on the attosecond timescale, *Phys. Rev. Lett.* 106(14), 143002 (2011)
8. J. M. Dahlström, A. L'Huillier, and A. Maquet, Introduction to attosecond delays in photo ionization, *J. Phys. B* 45(18), 183001 (2012)
9. J. M. Dahlström, D. Guenot, K. Klunder, M. Gisselbrecht, J. Mauritsson, A. L'Huillier, A. Maquet, and R. Taieb, Theory of attosecond delays in laser-assisted photo ionization, *Chem. Phys.* 414, 53 (2013)
10. A. S. Kheifets, Time delay in valence-shell photo ionization of noble-gas atoms, *Phys. Rev. A* 87(6), 063404 (2013)
11. A. Mandal, P. C. Deshmukh, A. S. Kheifets, V. K. Dolmatov, and S. T. Manson, Angle-resolved Wigner time delay in atomic photo ionization: The 4d subshell of free and confined Xe, *Phys. Rev. A* 96(5), 053407 (2017)
12. J. Watzel, A. S. Moskalenko, Y. Pavlyukh, and J. Berakdar, Angular resolved time delay in photoemission, *J. Phys. B* 48(2), 025602 (2015)
13. D. Guénot, D. Kroon, E. Balogh, E. W. Larsen, M. Kotur, M. Miranda,T. Fordell, P. Johnsson, J. Mauritsson, M. Gisselbrecht, K. Varjù, C. L. Arnold, T. Carette, A. S. Kheifets, E. Lindroth, A. L'Huillier, and J. M. Dahlström, Measurements of relative photoemission time delays in noble gas atoms, *J. Phys. B* 47(24), 245602 (2014)
14. J. Vos, L. Cattaneo, S. Patchkovskii, T. Zimmermann, C. Cirelli, M. Lucchini, A. Kheifets, A. S. Landsman, and U. Keller, Orientation-dependent stereo Wigner time delay and electron localization in a small molecule, *Science* 360(6395), 1326 (2018)
15. C. Cirelli, C. Marante, S. Heuser, C. L. M. Petersson, A. J. Galan, L. Argenti, S. Zhong, D. Busto, M. Isinger, S. Nandi, S. Maclot, L. Rading, P. Johnsson, M. Gisselbrecht, M. Lucchini, L. Gallmann, J. M. Dahlström, E. Lindroth, A. L'Huillier, F. Martín, and U. Keller, Anisotropic photoemission time delays close to a Fano resonance, *Nat. Commun.* 9(1), 955 (2018)
16. D. M. Villeneuve, P. Hockett, M. J. J. Vrakking, and H. Niikura, Coherent imaging of an attosecond electron wave packet, *Science* 356(6343), 1150 (2017)
17. S. Heuser, Á. Jiménez Galán, C. Cirelli, C. Marante, M. Sabbar, R. Boge, M. Lucchini, L. Gallmann, I. Ivanov, A. S. Kheifets, J. M. Dahlström, E. Lindroth, L. Argenti, F. Martín, and U. Keller, Angular dependence of photoemission time delay in helium, *Phys. Rev. A* 94(6), 063409 (2016)
18. P. Hockett, Angle-resolved RABBITT: Theory and numerics, *J. Phys. B* 50(15), 154002 (2017)
19. I. A. Ivanov and A. S. Kheifets, Angle-dependent time delay in two-color XUV+IR photoemission of he and ne, *Phys. Rev. A* 96(1), 013408 (2017)

20. A. W. Bray, F. Naseem, and A. S. Kheifets, Simulation of angular-resolved rabbitt measurements in noble gas atoms, *Phys. Rev. A* 97(6), 063404 (2018)
21. A. Harth, N. Douguet, K. Bartschat, R. Moshammer, and T. Pfeifer, Extracting phase information on continuum-continuum couplings, *Phys. Rev. A* 99(2), 023410 (2019)
22. J. Fuchs, N. Douguet, S. Donsa, F. Martin, J. Burgdorfer, L. Argenti, L. Cattaneo, and U. Keller, Time delays from one-photon transitions in the continuum, *Optica* 7(2), 154 (2020)
23. L. J. Zipp, A. Natan, and P. H. Bucksbaum, Probing electron delays in above-threshold ionization, *Optica* 1(6), 361 (2014)
24. X. Gong, C. Lin, F. He, Q. Song, K. Lin, Q. Ji, W. Zhang, J. Ma, P. Lu,Y. Liu, H. Zeng, W. Yang, and J. Wu, Energy-resolved ultrashort delays of photoelectron emission clocked by orthogonal two-color laser fields, *Phys. Rev. Lett.*118(14), 143203 (2017)
25. X. Song, G. Shi, G. Zhang, J. Xu, C. Lin, J. Chen, and W. Yang, Attosecond time delay of retrapped resonant ionization, *Phys. Rev. Lett.* 121(10), 103201 (2018)
26. A. Kramo, E. Hasovic, D. B. Milosevic, and W. Becker, Above-threshold detachment by a two-color bicircular laser field, *Laser Phys. Lett.* 4(4), 279 (2007)
27. C. A. Mancuso, D. D. Hickstein, P. Grychtol, R. Knut, O. Kfir, X. M. Tong, F. Dollar, D. Zusin, M. Gopalakrishnan, C. Gentry, E. Turgut, J. L. Ellis, M. C. Chen, A. Fleischer, O. Cohen, H. C. Kapteyn, and M. M. Murnane, Strong-field ionization with two-color circularly polarized laser fields, *Phys. Rev. A* 91(3), 031402 (2015)
28. C. A. Mancuso, D. D. Hickstein, K. M. Dorney, J. L. Ellis, E. Hasovic,R. Knut, P. Grychtol, C. Gentry, M. Gopalakrishnan, D. Zusin, F. J. Dollar, X. M. Tong, D. B. Milošević, W. Becker, H. C. Kapteyn, and M. M. Murnane, Controlling electron–ion rescattering in two-color circularly polarized femtosecond laser fields, *Phys. Rev. A* 3(5), 053406 (2016)
29. M. Ilchen, N. Douguet, T. Mazza, A. J. Rafipoor, C. Callegari, P. Finetti, O. Plekan, K. C. Prince, A. Demidovich, C. Grazioli, L. Avaldi, P. Bolognesi, M. Coreno, M. Di Fraia, M. Devetta, Y. Ovcharenko, S. Düsterer, K. Ueda, K. Bartschat, A. N. Grum-Grzhimailo, A. V. Bozhevolnov, A. K. Kazansky, N. M. Kabachnik, and M. Meyer, Circular dichroism in multiphoton ionization of resonantly excited He^+ ons, *Phys. Rev. Lett.* 118(1), 013002 (2017)
30. M. Busuladžić, A. Gazibegović-Busuladžić, and D. B. Milošević, Strong-field ionization of homonuclear diatomic molecules by a bicircular laser field: Rotational and reflection symmetries, *Phys. Rev. A* 5(3), 033411 (2017)
31. S. Eckart, K. Fehre, N. Eicke, A. Hartung, J. Rist, D. Trabert, N. Strenger, A. Pier, L. Ph. H. Schmidt, T. Jahnke, M. S. Schoffler, M. Lein,M. Kunitski, and R. Dorner, Direct experimental access to the nonadiabatic initial momentum offset upon tunnel ionization, *Phys. Rev. Lett.* 121(16), 163202 (2018)
32. M. Han, P. Ge, Y. Shao, Q. Gong, and Y. Liu, Attoclock photoelectron interferometry with two-color corotating circular fields to probe the phase and the amplitude of emitting wave packets, *Phys. Rev. Lett.* 120(7), 073202 (2018)
33. M. Li, W. C. Jiang, H. Xie, S. Luo, Y. Zhou, and P. Lu, Strong-field photoelectron holography of atoms by bicircular two-color laser pulses, *Phys. Rev. A* 97(2), 023415 (2018)
34. P. Ge, M. Han, Y. Deng, Q. Gong, and Y. Liu, Universal description of the attoclock with two-color corotating circular fields, *Phys. Rev. Lett.* 122(1), 013201 (2019)
35. Q. Ke, Y. Zhou, J. Tan, M. He, J. Liang, Y. Zhao, M. Li, and P. Lu, Two-dimensional photoelectron holography in strong-field tunneling ionization by counter rotating two-color circularly polarized laser pulses, *Opt. Express* 27(22), 32193 (2019)
36. T. N. Rescigno and C. W. McCurdy, Numerical grid methods for quantum–mechanical scattering problems, *Phys. Rev. A* 62(3), 032706 (2000)
37. W. C. Jiang and X. Q. Tian, Efficient split-lanczos propagator for strong-field ionization of atoms, *Opt. Express* 25(22), 26832 (2017)
38. J. Liang, W. C. Jiang, S. Wang, M. Li, Y. Zhou, and P. Lu, Atomic dynamic interference in intense linearly and circularly polarized XUV pulses, *J. Phys. B* 53(9), 095601 (2020)
39. S. Eckart, D. Trabert, K. Fehre, A. Geyer, J. Rist, K. Lin, F. Trinter, L. Ph. H. Schmidt, M. S. Schoffler, T. Jahnke, M. Kunitski, and R. Dorner, Sideband modulation by subcycle interference, *Phys. Rev. A* 102(4), 043115 (2020)
40. M. Wickenhauser, X. M. Tong, and C. D. Lin, Laser induced substructures in above-threshold-ionization spectra from intense few-cycle laser pulses, *Phys. Rev. A* 73, 011401(R) (2006)
41. A. Tóth and A. Csehi, Probing strong-field two-photon transitions through dynamic interference, *J. Phys. At. Mol. Opt. Phys.* 54(3), 035005 (2021)
42. Y. Feng, M. Li, S. Luo, K. Liu, B. Du, Y. Zhou, and P. Lu, Semiclassical analysis of photoelectron interference in a synthesized two-color laser pulse, *Phys. Rev. A* 100(6), 063411 (2019)
43. A. Jiménez-Galán, F. Martin, and L. Argenti, Two photon finite-pulse model for resonant transitions in attosecond experiments, *Phys. Rev. A* 93(2), 023429 (2016)
44. U. Fano, Propensity rules: An analytical approach, *Phys. Rev. A* 32(1), 617 (1985)
45. D. Busto, J. Vinbladh, S. Zhong, M. Isinger, S. Nandi, S. Maclot, P. Johnsson, M. Gisselbrecht, A. L'Huillier, E. Lindroth, and J. M. Dahlström, Fano's propensity rule in angle-resolved attosecond pump-probe photo ionization, *Phys. Rev. Lett.* 123(13), 133201 (2019)
46. A. R. Edmonds, Angular Momentum in Quantum Mechanics, Princeton, NJ: Princeton University Press, 1974
47. https://ww2.mathworks.cn/help/gads/ga.html
48. M. Bertolino and J. M. Dahlström, Multiphoton interaction phase shifts in attosecond science, *Phys. Rev. Res.* 3(1), 013270 (2021)
49. D. Bharti, D. Atri-Schuller, G. Menning, K. R. Hamilton, R. Moshammer,T. Pfeifer, N. Douguet, K. Bartschat, and A. Harth, Decomposition of the transition phase in multi-sideband schemes for reconstruction of attosecond beating by interference of two-photon transitions, *Phys. Rev. A* 103(2), 022834 (2021)